



Chinese Pharmaceutical Association
Institute of Materia Medica, Chinese Academy of Medical Sciences

Acta Pharmaceutica Sinica B

www.elsevier.com/locate/apsb
www.sciencedirect.com



ORIGINAL ARTICLE

Mevalonate improves anti-PD-1/PD-L1 efficacy by stabilizing *CD274* mRNA



Wenxin Zhang^{a,†}, Xiaohui Pan^{a,†}, Yanjun Xu^b, Hongjie Guo^a,
Mingming Zheng^a, Xi Chen^a, Honghai Wu^a, Fengming Luan^c,
Qiaojun He^{a,d,e}, Ling Ding^{a,*}, Bo Yang^{a,d,*}

^aZhejiang Province Key Laboratory of Anti-Cancer Drug Research, Institute of Pharmacology and Toxicology, College of Pharmaceutical Sciences, Zhejiang University, Hangzhou 310058, China

^bDepartment of Medical Thoracic Oncology, the Cancer Hospital of University of Chinese Academy of Sciences (Zhejiang Cancer Hospital), Chinese Academy of Sciences, Hangzhou 310022, China

^cDepartment of Gastrointestinal Surgery, Second Affiliated Hospital of Zhejiang University, School of Medicine, Hangzhou 310009, China

^dThe Innovation Institute for Artificial Intelligence in Medicine, Zhejiang University, Hangzhou 310018, China

^eCancer Center of Zhejiang University, Hangzhou 310058, China

Received 16 January 2023; received in revised form 27 February 2023; accepted 2 March 2023

KEY WORDS

Metabolites;
Mevalonate;
PD-L1;
mRNA stability;
HuR;
NSCLC;
Immune checkpoint
blockade

Abstract Mevalonate metabolism plays an important role in regulating tumor growth and progression; however, its role in immune evasion and immune checkpoint modulation remains unclear. Here, we found that non-small cell lung cancer (NSCLC) patients with higher plasma mevalonate response better to anti-PD-(L)1 therapy, as indicated by prolonged progression-free survival and overall survival. Plasma mevalonate levels were positively correlated with programmed death ligand-1 (PD-L1) expression in tumor tissues. In NSCLC cell lines and patient-derived cells, supplementation of mevalonate significantly up-regulated the expression of PD-L1, whereas deprivation of mevalonate reduced PD-L1 expression. Mevalonate increased *CD274* mRNA level but did not affect *CD274* transcription. Further, we confirmed that mevalonate improved *CD274* mRNA stability. Mevalonate promoted the affinity of the AU-rich element-binding protein HuR to the 3'-UTR regions of *CD274* mRNA and thereby stabilized *CD274* mRNA. By *in vivo* study, we further confirmed that mevalonate addition enhanced the anti-tumor effect of anti-PD-L1, increased the infiltration of CD8⁺ T cells, and improved cytotoxic function of T cells. Collectively, our findings discovered plasma mevalonate levels positively correlated with the therapeutic

*Corresponding authors. Tel./fax: +86 571 88208400.

E-mail addresses: yang924@zju.edu.cn (Bo Yang), ld362@zju.edu.cn (Ling Ding).

†These authors made equal contributions to this work.

Peer review under the responsibility of Chinese Pharmaceutical Association and Institute of Materia Medica, Chinese Academy of Medical Sciences.

<https://doi.org/10.1016/j.apsb.2023.04.002>

2211-3835 © 2023 Chinese Pharmaceutical Association and Institute of Materia Medica, Chinese Academy of Medical Sciences. Production and hosting by Elsevier B.V. This is an open access article under the CC BY-NC-ND license (<http://creativecommons.org/licenses/by-nc-nd/4.0/>).

efficacy of anti-PD-(L)1 antibody, and provided the evidence that mevalonate supplementation could be an immunosensitizer in NSCLC.

© 2023 Chinese Pharmaceutical Association and Institute of Materia Medica, Chinese Academy of Medical Sciences. Production and hosting by Elsevier B.V. This is an open access article under the CC BY-NC-ND license (<http://creativecommons.org/licenses/by-nc-nd/4.0/>).

1. Introduction

Metabolites have emerged as regulators for immune cells function and cancer immunogenicity¹. Accumulated evidence indicates that lactate² and prostaglandin E2³ polarize tumor microenvironment (TME) towards a more immunosuppressive characteristic by inhibiting natural killer (NK) cells function^{4,5}, inducing CD8⁺ T cells exhaustion^{6,7} and increasing immunosuppressive regulatory T cells recruitment^{8,9}. Blocking the production of lactate and prostaglandin E2 has been proved to be effective strategies for improved anti-PD-(L)1 efficacy. Supplementation of arginine promotes T cells and NK cells cytotoxicity and significantly enhances anti-tumor immune response of anti-PD-(L)1 treatment¹⁰. Pantothenate is demonstrated to reprogram T cells by increasing oxidative phosphorylation and adopting the CD8⁺ Tc22 phenotype. Supplementation of pantothenate is associated with increased T cell anti-tumor immunity, thereby enhanced response to anti-PD-L1 therapy¹¹. Furthermore, recent studies report lactate^{6,12} and prostaglandin E2^{13,14} up-regulate the immune molecules including programmed death ligand-1 (PD-L1), hindering their metabolism is an effective synergistic strategy for the immune checkpoint blockade. Inhibition of glutamine utilization increases PD-L1 expression in cancer cells, combined treatment with glutamine utilization inhibitor and anti-PD-L1 antibody indicates a synergistic anti-tumor effect¹⁵. NAD⁺ is recently identified to maintain the expression of PD-L1 in cancer cells. NAD⁺ replenishment sensitizes anti-PD-(L)1 treatment *in vivo*¹⁶. Taken together, these findings suggest that metabolic intervention can reshape the TME and boost the immune system which may serve as a promising approach to improve the efficacy of immunotherapy.

Mevalonate (MVA) is an upstream metabolite in the MVA pathway, which utilizes acetyl-CoA to produce cholesterol and isoprenoid metabolites under the action of various metabolic enzymes, and plays an indispensable role in regulating tumor growth and progression. Recently, the importance of MVA and its pathway-derived metabolites in cancer has been increasingly appreciated¹⁷. Cholesterol, MVA metabolism derivatives, is involved in membrane biogenesis, which is critical for highly proliferative cancer cells. Inhibition of cholesterol production alters fluidity or prevents lipid raft formation. Furthermore, MVA metabolism also plays an important role in the post-translational modification of proteins. Isoprenoids, including farnesyl diphosphate and geranylgeranyl diphosphate, are essential for the prenylation of small G proteins, thus inhibiting cancer cell growth and migration¹⁸. Dolichol is considered as a critical component of the *N*-glycosylation of nascent polypeptides in the endoplasmic reticulum¹⁹, and can contribute to cancer proliferation and metastasis. Apart from the above, MVA metabolism has been reported recently to modulate the effector functions of immune cells in TME. Farnesyl diphosphate and geranylgeranyl diphosphate are demonstrated to be associated with T cell immune

synapses formation, proliferation and cytotoxic functions^{20,21}. Cholesterol accumulation in the TME is considered to suppress T cell function^{22,23}. Accumulating evidence has demonstrated the critical role of MVA in tumor initiation and progression, the importance of MVA in regulating tumor immune evasion and immune response remains poorly understood.

Through untargeted metabolomics detection of blood samples from clinical non-small cell lung cancer (NSCLC) patients, we found that the peripheral MVA was correlated with the therapeutic efficacy of PD-(L)1 checkpoint blockade in NSCLC patients. Patients with higher MVA levels had better survival than those with lower plasma levels, as indicated by longer progression-free survival (PFS) and overall survival (OS). Further analysis revealed that patients with high peripheral MVA generally had higher PD-L1 expression in tumor. Mechanistically, MVA up-regulated PD-L1 expression by improving the stability of *CD274* mRNA. MVA increased the binding ability of the AU-rich elements (ARE)-binding protein human antigen R (HuR) to *CD274* mRNA 3'-UTR region, and thereby stabilized *CD274* mRNA in tumor cells. *In vivo* study also showed that MVA supplementation up-regulated PD-L1 expression in tumor cells and enhanced the anti-tumor efficacy of anti-PD-L1 therapy. Our findings indicated that plasma MVA is positively correlated with PD-L1 expression in tumor and the efficacy of anti-PD-(L)1 therapy. Moreover, our study raised the possibility that MVA replenishment combined with PD-(L)1 checkpoint blockade represents a promising therapeutic strategy for NSCLC immunotherapy.

2. Materials and methods

2.1. Antibodies

The following antibodies were used in immunoblotting: rabbit anti-B7-H3 (#14058), rabbit anti-PD-L1 (#13684), rabbit anti-CD86 (#91882), rabbit anti-CD47 (#63000), rabbit anti-Phospho-Stat1 (Tyr701) (#9167), rabbit anti-Phospho-Stat1 (Ser727) (#8826) and rabbit anti-Phospho-Stat3 (Tyr705) (#9145) were purchased from Cell Signaling Technology (Boston, USA). Rabbit anti-Stat1 (10144-2-AP), rabbit anti-Stat3 (10253-2-AP), rabbit anti-HuR (11910-1-AP), rabbit anti-HMGCR (13533-1-AP) and rabbit anti-TTP (12737-1-AP) were from Proteintech (Chicago, USA). Mouse anti-Galectin-9 (ab153673, abcam, Cambridge, UK), rabbit anti-GAPDH (db106, Diagbio, Hangzhou, China), goat anti-mouse PD-L1 (AF1019, R&D systems, Minnesota, USA). The antibodies for flow cytometry: FITC Rat IgG2b κ isotype control (#400605), FITC Rat IgG2a κ isotype control (#400506), PE Rat IgG2a λ isotype control (#400635), PE anti-mouse PD-L1 (#124307), FITC anti-mouse CD3 (#100204), FITC anti-mouse CD8a (#100705) and PE anti-mouse CD45 (#103106) were from Biolegend (Chicago, USA).

2.2. Reagents

Rosuvastatin (T1676), Pravastatin (T22405), Simvastatin (T0687), Fluvastatin (T1487), Pitavastatin (T2534), MG132 (T2154) and chloroquine (T8689) were purchased from TargetMol (Shanghai, China). Human IFN γ was purchased from PeproTech China (#300-02-1000, China) and mouse IFN γ was obtained from SinoBiological (50709-MNAH, Beijing, China). Mevalonic acid lithium salt (#90469) and cycloheximide (#239763-M) were from Sigma–Aldrich (Saint Louis, MO, USA). Actinomycin D was obtained from Selleck (S8964, Houston, TX, USA). Mevalonic acid lithium salt administrated *in vivo* was purchased from Med-ChemExpress (HY-113071A, NJ, USA), and anti-mouse PD-L1 antibody *in vivo* was purchased from BioXcell (BE0101, West Lebanon, NY, USA). D,L-Mevalonolactone-4,4,5,5-*d*₄ (>99%) for LC–MS/MS detection was purchased from CDN Isotopes (Pointe-Claire, Quebec, Canada).

2.3. Cell culture

All the cell lines were kindly provided by Cell Bank of Shanghai Institutes for Biological Sciences, Chinese Academy of Sciences (Shanghai, China). All cell lines were tested and verified to be free of mycoplasma. NCI-H292, NCI-H460, NCI-H358, NCI-H838, NCI-H1975, HCC827, CT26, SW620, 786-O and 769-P were cultured in RPMI-1640 (#31800, Gibco, LA, USA) supplemented with 10% fetal bovine serum (FBS; SV30160.03, Hyclone, GE Healthcare, USA). HEK 293FT and A2058 were maintained in DMEM (#12800, Gibco, LA, USA) with 10% FBS. All cell lines were cultured in a humidified incubator at 37 °C in a 5% CO₂.

2.4. Primary cancer cells isolation

Fresh cancer tissues of NSCLC patients were obtained with the donor's written consent and approved by Zhejiang Cancer Hospital Committee (IRB-2019-175). The cancer tissues were cut and dissociated into rice-grain-sized blocks *via* sterilized surgical instruments after cleaning twice with RPMI-1640. Then, the cancer blocks were placed in T25 culture flasks containing DMEM/F-12 (10565018, Gibco, LA, USA) with 20% FBS. Subsequently, fresh culture medium was changed every 2 days until primary cancer cells were crawled out of the tissue. Cells were then maintained in a humidified incubator at 37 °C in a 5% CO₂.

2.5. Clinical blood samples and tumor tissues collection

NSCLC patients were enrolled for treatment with nivolumab (3 mg/kg, once every two weeks), and patients' blood samples and tumor paraffin sections were collected at Zhejiang Cancer Hospital after approval by the ethics committee and Institutional Review Board of Zhejiang Cancer Hospital (IRB-2019-175). Written consent was obtained from each NSCLC patient before blood and tumor tissue collection, and the experiments were performed in accordance with relevant ethical regulations.

2.6. Immunohistochemistry staining

All cancer tissue specimens were incubated with 3% H₂O₂ (PV-6001, ZSGB-BIO, Beijing, China) for 15 min and blocked by staining with blocking buffer contained 5% goat serum (#16210064, Gibco) for 30 min. Sections were treated with primary antibodies against PD-L1 (1:100) at 4 °C overnight. Sections

were then incubated with HRP-conjugated secondary antibodies (PV-6001/2, ZSGB-BIO, Beijing, China) for 1 h at room temperature, followed by treated with an avidin–biotin–peroxidase complex and developed with 3,3-diaminobenzidine as protocol by manufacture. Images were taken using an Olympus microscopic, and were scanned on Image-Pro Plus 6.0 software (IPP, version 6.0, Media Cybernetics) for quantification by digital image analysis. PD-L1 expression in tumor tissue specimens was computed from the intensity of the immunostaining as “–”, negative; “+”, weak staining; “++”, intermediate staining; “+++”, strong staining. The score less than 50% was considered as low expression and greater than 50% was considered as high expression as previously described²⁴.

2.7. Western blot

Cells were washed twice with cold PBS and lysed in 1% NP-40 buffer (25 mmol/L Tris-base, pH 7.4, 150 mmol/L NaCl, 10% glycerol). Equal amount of protein was separated by SDS-PAGE, and transferred to PVDF membranes. The blots were blocked in 5% non-fat milk for 1 h in room temperature, and incubated overnight at 4 °C with primary antibodies. After washing three times with PBST, the blots were incubated with HRP-conjugated secondary antibody. The protein bands were then developed with ECL detection reagents and analyzed by chemiluminescence imaging system (GE Amersham Imager 600, USA).

2.8. Flow cytometry

Cells were washed with cold PBS and stained with FITC-conjugated PD-L1 (or FITC isotype control) in 100 μ L 0.2% bovine serum albumin at 4 °C for 2 h (5 μ L/2 \times 10⁵ cells). After washing with cold PBS, samples were detected by BD FACSuite TM (BD bioscience, USA). Tumor tissues were minced and separated into single-cell through a tissue dissociator (Miltenyi Biotec, USA). Cells were then stained with antibodies against CD3, CD8a and CD45 in 100 μ L 0.2% bovine serum albumin at room temperature for 30 min (1 μ L/2 \times 10⁵ cells). Cells were washed with PBS and analyzed by flow cytometry. The data were analyzed by one-way ANOVA with Dunnett's *post hoc* test.

2.9. siRNA-mediated silencing

Cells were plated in 6-well plates for 24 h, then cells were transfected with transfection reagent INTERFERin (#409-10, Polyplus, France), Jet PRIME Buffer (#712-60, Polyplus, France) and *HMGCR* (*ELAVL1*, *KHSRP*, *DHX36*, *HNRNPD* and *ZFP36*) siRNA or siRNA-negative control (Jet PRIME buffer: 200 μ L; JetPRIME: 2 μ L; 20 μ mol/L siRNA: 2.5 μ L for per well) for 24 h. The siRNA sequences used in the study are listed in Supporting Information Table S1.

2.10. Plasmid construction

Cells were transfected with the indicated plasmids or empty vector by using transfected reagent JetPRIME (#114-15, Polyplus, France) according to the manufacturer's instructions. The mammalian expression vector pEnCMV-MCS-3 \times FLAG-WPRE-SV40-Neo (#P27576), the full-length of *HMGCR* (#P27213) and *ELAVL1* (#P20849) were obtained from Miao Ling Plasmid (Wuhan, China). Further, for the *CD274* promoter (#P7914), 3'-

UTR (#P24320) and 5'-UTR (#P37542) luciferase reporters were synthesized at Miao Ling Plasmid (Wuhan, China).

2.11. CRISPR/Cas9-mediated knockout of *Elavl1*

CRISPR/Cas9-mediated *Elavl1* knockout in CT26 cells were generated as previously described²⁴. Briefly, two targeted sgRNAs were obtained from CRISPR design tool <http://crispor.tefor.net/>, and the *Elavl1* sgRNA were constructed by inserting the targeted sgRNA into Px458 plasmid (#48138, Addgene, USA). To construct *Elavl1* knockout CT26 cells, cells were transfected with *Elavl1* sgRNA plasmid using indicated transfection reagent. After deriving the single cell by fluorescence-activated cell sorting, the successfully edited clones were determined by Western blot. The sgRNA sequences are listed as follows:

Elavl1 sgRNA1:

Sense (5'-3'): CACCGAAGACATGTTTCTCGGTT;
Antisense (5'-3'): AAACAACCGAGAAAACATGTCTTC;

Elavl1 sgRNA2:

Sense (5'-3'): CACCGTCTGAACGGCTACCGCCTG;
Antisense (5'-3'): AAACCAGCGGTAGCCGTTTCAGAC.

2.12. RNA isolation and quantitative real-time PCR

Total RNA was extracted using TRIzol reagent (#9109, TaKaRa, China), and further purified according to standard protocols. RNA was quantified by NanoDropND-1000 Spectrophotometer (ThermoFisher Scientific, USA) and synthesized into cDNA by using TransScript One-Step gDNA Removal and cDNA Synthesis SuperMix (#AT311-03, TRAN, China). Quantitative RT-PCR was performed with SYBR-Green kit (#172-5124, Bio-Rad, USA), and its accuracy was calculated using the comparative Ct method. *ACTB* was used as the normalizing gene. The primers used are provided as Supporting Information Table S2.

2.13. Nucleocytoplasmic separation

Cells were washed twice with cold PBS and lysed in 0.5% NP-40 buffer (0.5% NP-40, 100 mmol/L Tris-base, pH 8.4, 140 mmol/L NaCl, 1.5 mmol/L MgCl₂, 1 mmol/L DTT, 100 μL/5 × 10⁶ cells) for 5 min incubation on ice, followed by homogenization. After centrifugation, cytoplasmic fraction was the supernatant. The preliminary nuclear fraction was resuspended in IP buffer (10 mmol/L Tris-HCl, pH 7.4, 10 mmol/L NaCl, 3 mmol/L MgCl₂, 1 mmol/L DTT, 1% Triton X-100, 1% NP-40, 0.5 mmol/L PMSF). Following lysis on ice for 20 min, and then centrifugated at 13,500 × g for 30 min. After quantified using a BCA assay, the equal amount of protein was dissolved in loading buffer and electrophoresed on SDS-PAGE.

2.14. Luciferase reporter assay

Cells were co-transfected with *CD274* promoter (or 3'-UTR, 5'-UTR) luciferase reporter constructs and *Renilla*. After incubation for 24 h, the cells were washed with cold PBS and the reporter activities were assayed using the dual-luciferase reporter assay system (#E1910, Promega, USA) following the manufacturer's protocol. The *Renilla* luciferase plasmid (#E2231, Promega, USA)

was used as the internal control to normalize the transfection efficiency, and the results are expressed as relative luciferase activity (firefly luciferase/*Renilla* luciferase).

2.15. RNA-immunoprecipitation (RIP)

RIP reactions were carried out using Magna-RIP RNA-IP Kit (Millipore, USA) with normal rabbit IgG control, anti-rabbit-HuR or anti-rabbit-TTP antibodies according to the manufacturer's instructions. RNA was extracted using TRIzol, qPCR and qRT-PCR were performed as described above, and the % input method was used to calculate RNA enrichment.

2.16. ELISA assay of tumor cytokines

Mouse tumors were homogenized by stainless steel beads in 1% RIPA buffer (0.5% sodium deoxycholate, 50 mmol/L Tris-base, pH 7.4, 150 mmol/L NaCl, 1% Triton X-100 and 0.1% SDS). ELISA array was performed using the mouse IFN-γ (RK00019, ABclonal, China), mouse IL-2 (RK00007, ABclonal, China) and mouse TNF-α (RK00027, ABclonal, China) ELISA Kit according to the manufacturer's instructions.

2.17. Animal experiments

Animal procedures were conducted according to the guidelines approved by the Institutional Animal Care and Use Committee (IACUC#19-136, 19-262), and performed in light of protocols established by the Center for Drug Safety Evaluation and Research of Zhejiang University. CT26 tumors were constructed subcutaneously injecting CT26 cells (5 × 10⁵ per mouse in a 100 μL medium) into 6-week-old BALB/c male mice. Tumor volumes were measured every day with a caliper and calculated by Eq. (1):

$$\text{Tumor volume} = \text{Length} \times \text{Width}^2 \times 0.5 \quad (1)$$

Mice were pooled and randomly divided into four groups with comparable average tumor size. Mice were grouped into control (PBS), MVA addition (HY-113071A, MedChemExpress, USA), anti-mouse PD-L1 treatment (BE0101, BioXcell, USA) and MVA addition plus anti-mouse PD-L1 treatment. PBS or MVA were treated daily by intraperitoneal injection (100 mg/kg), and anti-mouse PD-L1 treatment was given twice a week by intravenous injection (5 mg/kg). Mice were euthanized 14 days after drug treatment or if the tumor volume exceeded 2000 mm³.

2.18. Untargeted metabolomic analysis

Plasma samples from 40 NSCLC patients were obtained before anti-PD-1 treatment. Untargeted metabolomic analysis were performed by Shanghai Applied Protein Technology Co., Ltd. (Shanghai, China). Briefly, to detect metabolites from plasma samples, 100 μL of each sample was added to pre-cooled methanol/acetonitrile/water solution (2:2:1, v/v/v), mixed by vortex, with 5 min incubation at 4 °C after each vortex step. After the final vortex step, the mixture was incubated on ice for 10 min. Then, 100 μL chilled HPLC-certified water was added to each sample and centrifuged at 13,000 × g for 10 min at 4 °C. Finally, the liquid phase (supernatant) of each sample was transferred into a new tube for UHPLC-QTOF-MS analysis. The data acquisition,

principal component analysis and pathway impact analysis were performed by Shanghai Applied Protein Technology Co., Ltd.

2.19. LC–MS/MS analysis of plasma MVA levels

A simple plasma extraction method coupled with LC–MS/MS detection for the endogenous MVA was described as before²⁵. Briefly, a 50 µg/mL stock solution of DL-mevalonolactone (MVL) was prepared in methanol. Prepared calibration standards and quality controls with 0.5 mmol/L sodium phosphate buffer. Then we added 100 µL of each standard, QC and plasma samples along with 10 µL of IS (²H₄-mevalonolactone, 100 ng/mL in water). This was followed by adding 200 µL of extraction buffer and 1000 µL ethylacetate to each sample. All tubes were shaken vigorously for 60 min and centrifuged at 4000 × *g* for 10 min at 4 °C. Transferred the upper organic supernatants to 800 µL ethylacetate and evaporated to dryness under nitrogen at 40 °C, reconstituted with 50 µL of 0.5% formic acid and finally performed the LC–MS/MS analysis.

2.20. Statistical analysis

Data are presented as the mean ± standard deviation (sd) of at least triplicate independent experiments and represented as percentage related to negative control or untreated groups. GraphPad Prism v.6.0 was performed for statistical analysis. Student's *t*-test was used to determine Statistical differences (two groups). The data were analyzed by one-way ANOVA with Dunnett's *post hoc* test (more than two groups). ****P* < 0.001; ***P* < 0.01; **P* < 0.05; ###*P* < 0.001; ##*P* < 0.01; #*P* < 0.05; n.s: not significant. For NSCLC patients' survival was evaluated by the Kaplan–Meier method. PFS and OS were analyzed by the Mantel–Cox log rank test.

2.21. Data availability

The data supporting this study is available in the article. Raw data for all figures and supplementary information have been provided as a source data file. Correlation between MVA pathway enzymes and cytotoxic cytokine-associated genes expression were obtained from <https://www.aclbi.com/>. The relative mRNA expression of MVA pathway enzymes in NSCLC cell lines were obtained from <https://depmap.org/portal/>.

3. Results

3.1. Plasma MVA positively correlates with effective anti-PD-(L)1 therapy in NSCLC

Given that a variety of metabolites have been demonstrated to be essential in T cell activation and immune response regulation^{16,26–29}. Searching for metabolites correlated to the clinical efficacy of immunotherapy draws great interests. Herein, we performed untargeted metabolomics detection in NSCLC patients treated with anti-PD-1 antibodies (Fig. 1A and Supporting Information Table S3). Peripheral blood samples for the assay were obtained before anti-PD-1 treatment. According to the clinical efficacy of NSCLC patients with anti-PD-1 therapy, patients with PFS > 6 months and OS > 6 months were categorized into long survival, while the rest were identified as short survival. Through differential analysis and cluster analysis of metabolites in

peripheral blood of long-surviving and short-surviving patients, we noted that MVA was significantly altered between two groups (Fig. 1B and C).

Next, we further analyzed whether plasma MVA levels were associated with NSCLC patients' immunotherapy efficacy. We used LC–MS/MS to measure the plasma MVA levels in NSCLC patients with anti-PD-1 treatment²⁵. Markedly, higher levels of MVA in plasma were found in long-surviving patients with immunotherapy, when compared with those of short survival (Fig. 1D). Patients with high MVA level showed a better response to anti-PD-1 therapy, with longer PFS and OS (Fig. 1E and F). Further, we separated NSCLC patients into three groups according to their plasma MVA levels: patients with low level of MVA (< 3 ng/mL), medium level of MVA (3–5 ng/mL), and high level of MVA (> 5 ng/mL) (Supporting Information Table S4). Patients with low level of MVA had more proportion of progressive disease (PD) and stable disease (SD) patients. On the contrary, high percentage of partial response (PR) and complete response (CR) patients were investigated in high plasma MVA levels. Patients with high plasma MVA levels had higher objective response rate (ORR) and disease control rate (DCR) (ORR 69.2% versus 27.7%; DCR 100% versus 66.7%) compared with low plasma MVA levels (Fig. 1G). Notably, age, gender and lung cancer type were not significantly different among the three groups (Fig. 1H). These data from pre-immunotherapy treatment of NSCLC patients' peripheral blood suggested that effective anti-PD-(L)1 therapy correlated with high plasma MVA levels.

3.2. Plasma MVA level is associated with high PD-L1 expression

A multitude of studies have confirmed the enhanced efficacy of anti-PD-(L)1 therapy in NSCLC patients with higher levels of tumor PD-L1 expression^{30,31}. We further evaluated the immunohistochemistry staining of PD-L1 in above cohort of patients with anti-PD-1 therapy (Supporting Information Fig. S1). Consistently, patients with higher PD-L1 expression indicated prolonged PFS and OS (Fig. 2A and B). To assess whether plasma MVA-indicated immunotherapy efficacy is associated with regulating tumor PD-L1 expression. We analyzed the correlation between plasma MVA levels in NSCLC patients and their PD-L1 expression in tumor tissues. As shown in Fig. 2C, we observed that patients with high plasma MVA levels generally had higher PD-L1 expression in their tumors, whereas patients with low plasma MVA levels had the opposite characteristic. PD-L1 is well known for inducing T cell dysfunction^{32,33}. Therefore, we analyzed the correlation between MVA pathway and cytotoxic cytokine-associated gene expression in CD8⁺ T cells³⁴. Notably, the expression of MVA pathway metabolic enzymes were negatively associated with expression of various cytotoxic cytokine-related genes (Fig. 2D). Collectively, these data suggested that plasma MVA positively correlates with anti-PD-(L)1 efficacy may due to regulation of PD-L1 expression.

3.3. MVA promotes PD-L1 expression in NSCLC cells

To further investigate the mechanism of high plasma MVA induced higher PD-L1 expression in patient's tumor tissues, we evaluated PD-L1 expression in NSCLC cell lines by depriving or supplementing MVA *in vitro*. The results showed that PD-L1 was significantly up-regulated by MVA supplementation, while

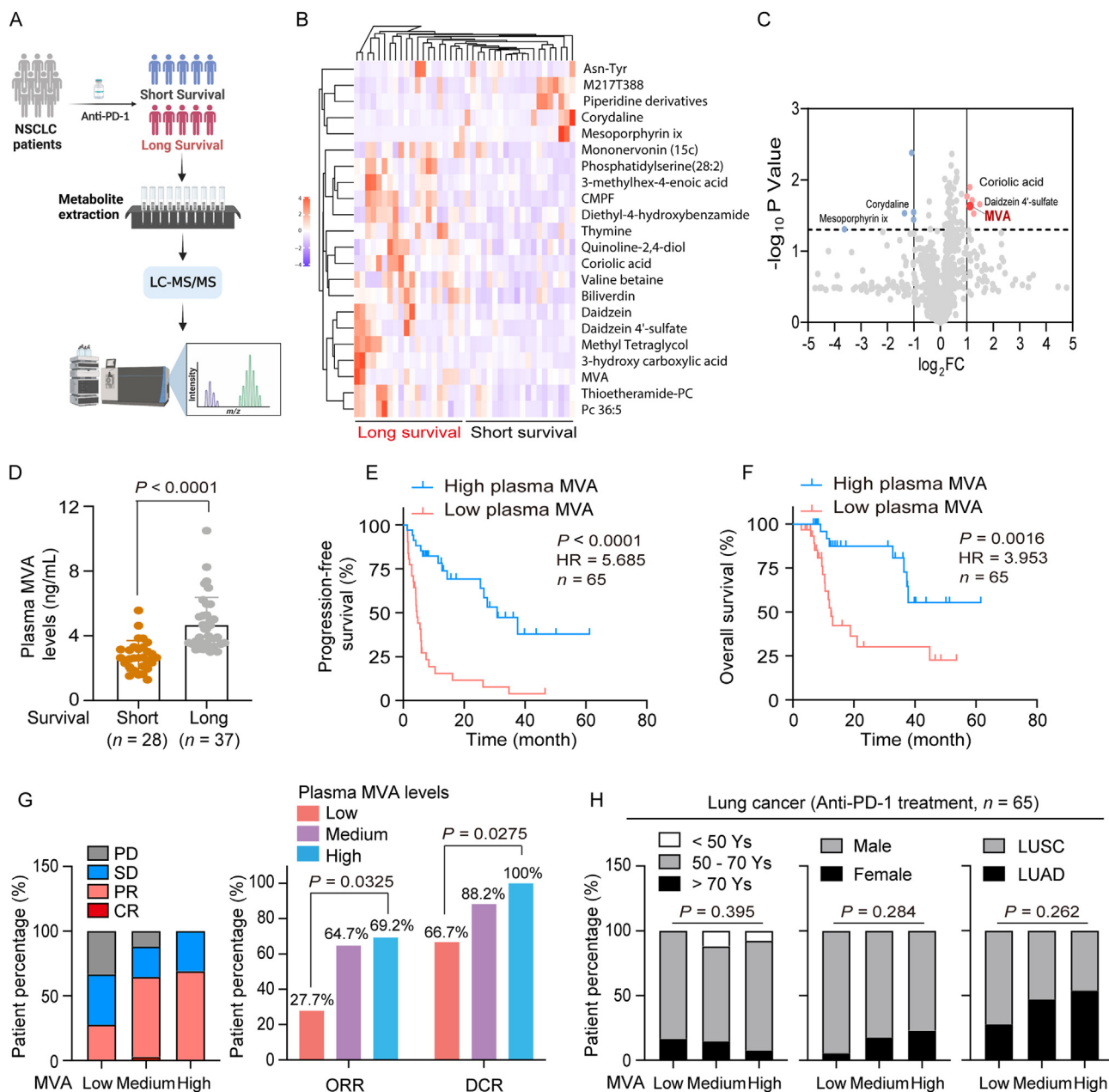


Figure 1 Plasma MVA positively correlates with effective anti-PD-(L)1 therapy in NSCLC. (A) Schematic illustration of untargeted metabolomics detection. 40 peripheral blood samples were obtained from NSCLC patients with anti-PD-1 therapy. The blood samples were collected before anti-PD-1 antibody treatment. (B) Significantly differential metabolite hierarchical clustering heatmap of patients with long survival (left) and short survival (right) of NSCLC. Significance was determined as a fold change of at least 1.5 and P value < 0.05 . Long survival ($n = 20$); Short survival ($n = 20$). (C) Volcano plot of differentially abundant metabolites in peripheral blood of long-surviving and short-surviving patients of NSCLC. Significance was determined as P value < 0.05 . (D) Comparison of plasma MVA levels from NSCLC patients with long or short survival after anti-PD-1 therapy. Student's t -test was performed to statistics significance of experimental data. Long survival ($n = 37$); Short survival ($n = 28$). (E, F) Kaplan-Meier plot of PFS and OS for patients with NSCLC stratified by high or low plasma MVA levels ($n = 65$). Top 50% plasma MVA levels were considered as high MVA levels. PFS and OS were compared using the log-rank test. (G) Different plasma MVA levels of NSCLC patients stratified by different clinical outcomes after anti-PD-1 therapy. CR, complete response; PR, partial response; SD, stable disease; PD, progressive disease. Assessment data of the ORR and DCR among NSCLC patients were performed using Fisher's exact test. (H) The distributions of age, gender and cancer type among patients with indicated MVA levels. Assessment data were performed using Fisher's exact test.

rosuvastatin inhibited PD-L1 expression. However, there was no significant difference in the expression of other immune checkpoint proteins (Fig. 3A). Further combined with CCLE database analysis, we added MVA in two NSCLC cell lines NCI-H838 and

NCI-H1975 with relatively low expression of MVA pathway enzymes, and increasing expression of PD-L1 was verified. In parallel, administration of rosuvastatin in two other NSCLC cell lines NCI-H460 and NCI-H358 with relatively high expression of

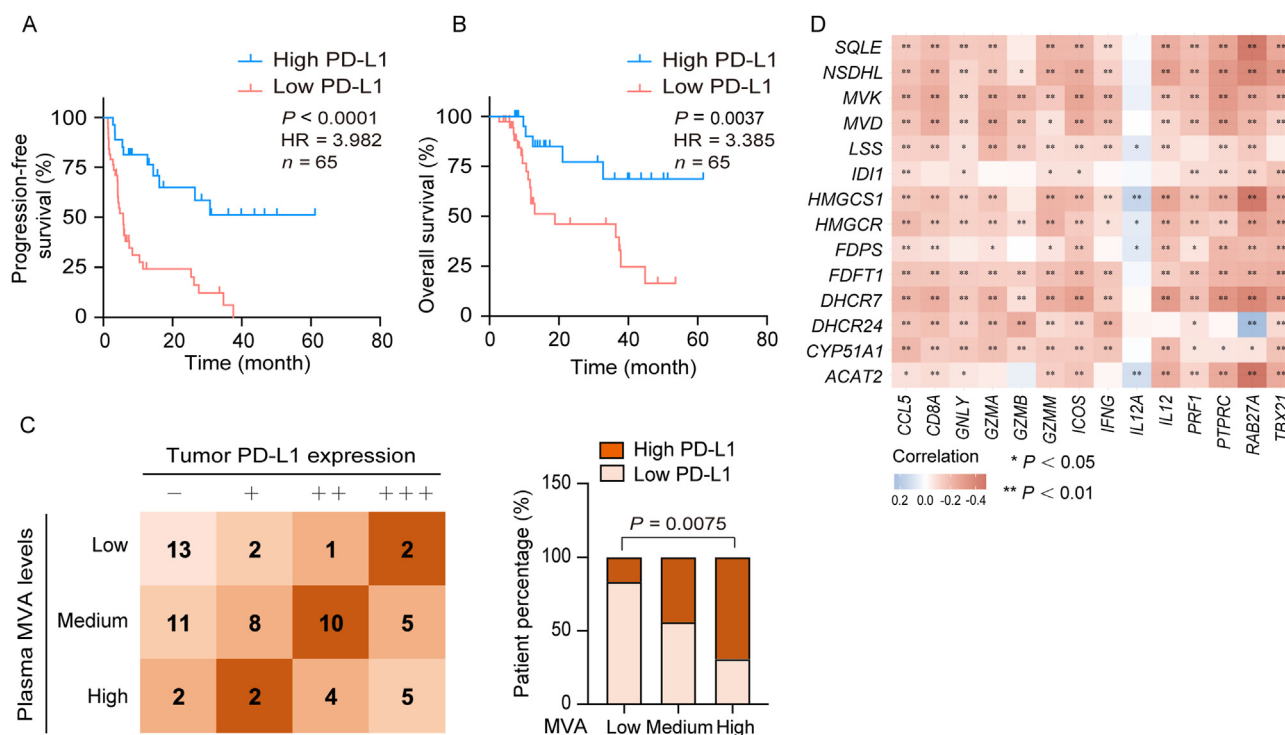


Figure 2 Plasma MVA levels are associated with tumor PD-L1 expression. (A, B) Kaplan–Meier plot of PFS and OS for patients of NSCLC were stratified by high (staining score 2–3) or low (staining score 0–1) PD-L1 expression in tumor tissues ($n = 65$). PFS and OS were compared using the log-rank test. (C) Tumor tissues from NSCLC patients with anti-PD-1 therapy were stained with PD-L1. –, negative expression, staining score 0; +, low expression, staining score 1; ++, medium expression, staining score 2; +++, high positive expression, staining score 3. Different plasma MVA levels of NSCLC patients were stratified by high or low PD-L1 expression. Assessment data were performed using Fisher’s exact test. (D) Correlation between MVA pathway metabolic enzymes and cytotoxic cytokine-associated genes expression in $CD8^+$ T cells by TCGA database. ** $P < 0.01$; * $P < 0.05$.

pathway enzymes inhibited PD-L1 expression (Fig. 3B and Supporting Information Fig. S2A). Consistently, we found that cell-surface PD-L1 expression was up-regulated with the addition of MVA (Fig. 3C). Because PD-L1 expression is mainly stimulated by interferon- γ (IFN γ) *in vivo*¹⁶, we examined the effect of Rosuvastatin under IFN γ -induced conditions. Similarly, rosuvastatin completely reduced PD-L1 expression induced by IFN γ (Fig. 3D and Fig. S2B). Then we deprived MVA by using statins, the 3-hydroxy-3-methylglutaryl-CoA reductase (HMGCR) inhibitors, and analyzed PD-L1 expression. The results show that statins could significantly down-regulate PD-L1 expression (Fig. S2C). Furthermore, HMGCR overexpression exhibited a remarkable PD-L1 up-regulation both at the total proteins and surface proteins (Fig. 3E), whereas HMGCR knockdown reduced PD-L1 expression (Fig. 3F). The efficacy of HMGCR overexpression or knockdown in tumor cells of flow cytometry analysis is shown in Fig. S2D. Moreover, addition of MVA could effectively reverse the decrease of PD-L1 expression caused by rosuvastatin treatment in NCI-H292 cells and five primary lung cancer cells (Fig. 3G and H). These results suggest that MVA was critical for PD-L1 expression in NSCLC. Furthermore, in order to investigate whether the regulation of MVA on PD-L1 expression also exist in other tumor cell lines, we administrated rosuvastatin alone or together with MVA in the colorectal cancer cell line SW620, melanoma cell line A2058, and renal cancer cell lines 786-O and 769-P. The results showed that rosuvastatin could down-regulate PD-L1 expression in the above cell lines, while

supplemented MVA completely reversed the inhibitory effect of rosuvastatin (Fig. S2E). These results suggest that the regulation of MVA on PD-L1 expression was not limited to NSCLC.

3.4. MVA improves CD274 mRNA stability

To understand the mechanism of MVA induced PD-L1 up-regulation, we measured the mRNA levels and protein half-life of PD-L1 in response to MVA supplementation. The qRT-PCR results showed that MVA significantly increased CD274 mRNA levels, while statins effectively suppressed CD274 mRNA levels (Fig. 4A and Supporting Information Fig. S3A). Similar observation was obtained when HMGCR was overexpressed or knocked down (Fig. 4B). We excluded the impact of MVA on PD-L1 protein stability by analyzing the half-life of PD-L1 protein (Fig. S3B), while there was no significant difference in the rate of PD-L1 protein degradation was observed. Consistent with the results from protein stability experiment, both proteasome pathway inhibitor MG132 and lysosomal pathway inhibitor chloroquine couldn’t rescue the decrease of PD-L1 expression treated with rosuvastatin (Fig. S3C).

Given that signal transducer and activator of transcription 1 (STAT1)^{16,35} and STAT3³⁶ are critical in CD274 transcription^{37,38}, we analyzed whether MVA affected the activity of these transcription factors. The data showed that rosuvastatin did not affect the phosphorylation of STAT1 and STAT3 induced by IFN γ in NCI-H292 cells, while PD-L1 expression was consistently inhibited

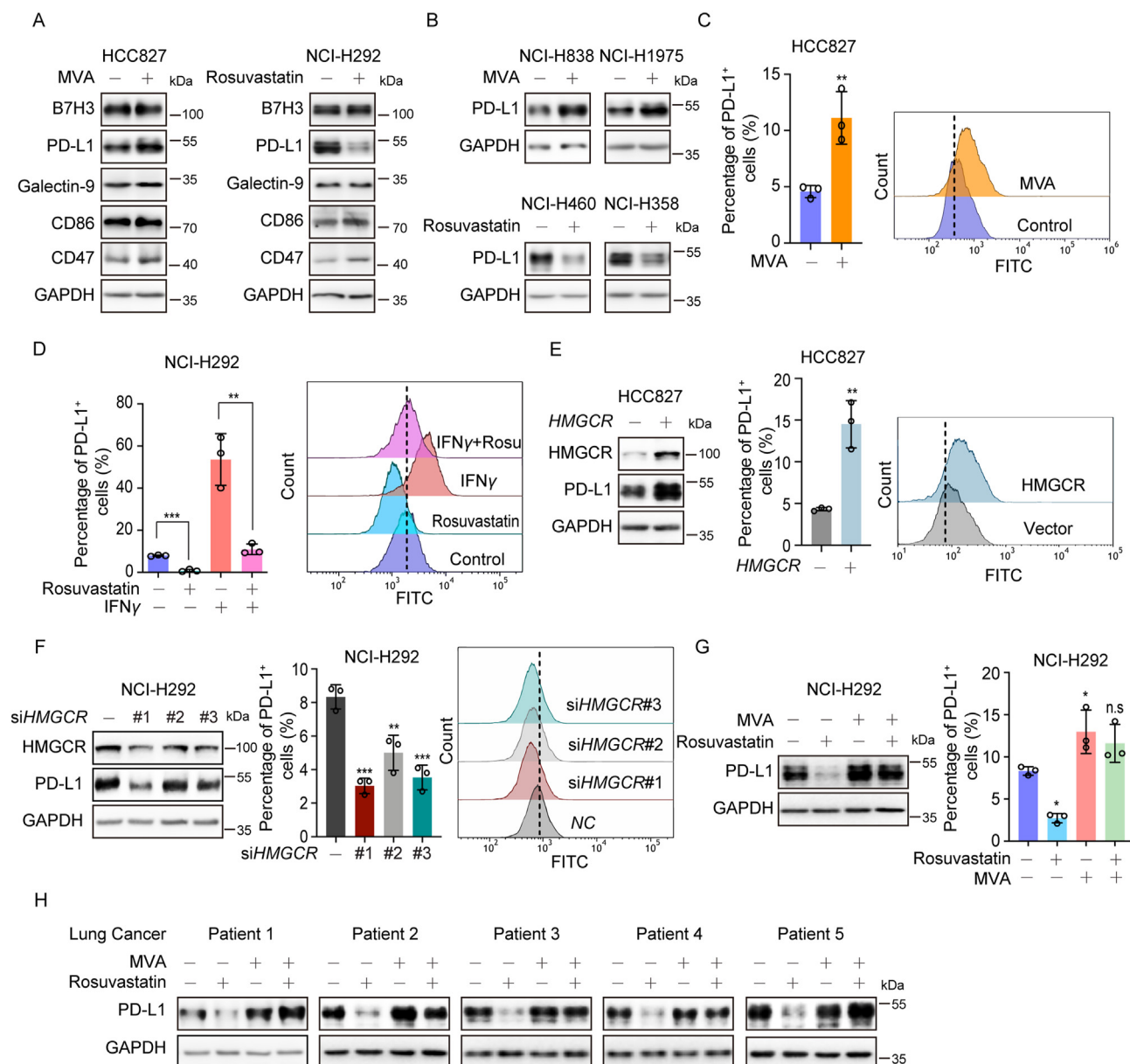


Figure 3 MVA promotes PD-L1 expression in NSCLC cells. (A) Western blot of B7H3, PD-L1, Galectin-9, CD86, and CD47 in NSCLC cell lines HCC827 (left) treated with MVA (0.5 mmol/L) and NCI-H292 (right) treated with rosuvastatin (10 μ mol/L). (B) Western blot of PD-L1 in NSCLC cell lines treated with MVA (0.5 mmol/L) or rosuvastatin (10 μ mol/L). NCI-H838 and NCI-H1975 cells (top) represent low expression of MVA pathway enzymes, while NCI-H460 and NCI-H358 cells (bottom) represent high expression. (C, D) Flow cytometry analysis of cell-surface PD-L1 expression in HCC827 (C) with MVA (0.5 mmol/L) and NCI-H292 (D) with IFN γ (10 ng/mL) and rosuvastatin (10 μ mol/L). (E, F) Western blot (left) and flow cytometry analysis (right) of PD-L1 expression in cells with HMGCR overexpression (E) and knockdown (F). (G) Western blot (left) and flow cytometry analysis (right) of PD-L1 expression in cells after treatment with rosuvastatin (10 μ mol/L), MVA (0.5 mmol/L), or both. (H) Western blot of PD-L1 expression in five human primary lung cancer cells with rosuvastatin (10 μ mol/L), MVA (0.5 mmol/L), or both. Data are presented as the mean \pm sd of triplicate independent experiments. Student's *t*-test was used to determine statistical differences (two groups). The data were analyzed by one-way ANOVA with Dunnett's *post hoc* test (more than two groups). ****P* < 0.001; ***P* < 0.01; **P* < 0.05; n.s., not significantly different.

(Fig. 4C). Similarly, addition of MVA up-regulated PD-L1 expression without affecting the phosphorylation of STAT1 and STAT3 induced by IFN γ in HCC827 cells (Fig. S3D). By nucleocytoplasmic separation assay, we also confirmed that the rosuvastatin did not affect the nucleocytoplasmic shuttling process of *CD274* transcription factors STAT1 and STAT3 (Fig. 4D). Then, we generated a

luciferase reporter construct containing 2000 bp region of human *CD274* promoter, and used luciferase assay to investigate the effect of MVA and rosuvastatin administration on *CD274* transcription. No significant change of *CD274* promoter activity was found (Fig. 4E). Collectively, these data all suggest that MVA caused *CD274* mRNA increase was not due to transcription promotion.

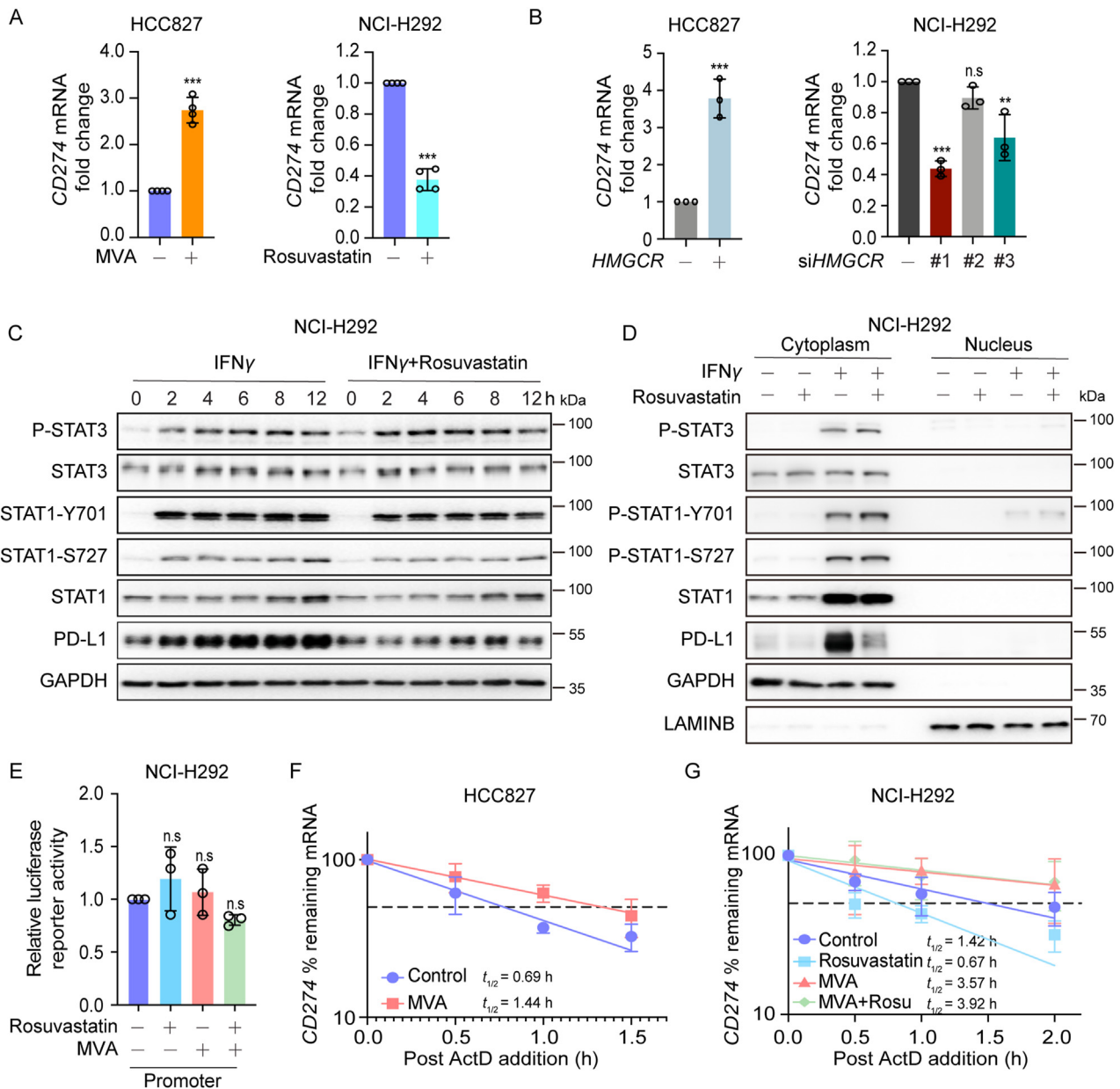


Figure 4 MVA improves *CD274* mRNA stability. (A) qRT-PCR analysis of *CD274* mRNA levels in HCC827 (left) treated with MVA (0.5 mmol/L) and NCI-H292 (right) treated with rosuvastatin (10 μ mol/L). (B) qRT-PCR analysis of *CD274* mRNA levels in cells with transient HMGCR overexpression (left) or knockdown (right). (C) The expression of P-STAT3, STAT3, P-STAT1(Y701), P-STAT1(S727), STAT1 and PD-L1 proteins in NCI-H292 cells with or without rosuvastatin (10 μ mol/L) in the presence of IFN γ (10 ng/mL) for 0, 2, 4, 6, 8, and 12 h were assessed by Western blot. (D) The P-STAT3, STAT3, P-STAT1(Y701), P-STAT1(S727), STAT1 and PD-L1 proteins in cytoplasm and nucleus were determined when cells were treated with rosuvastatin (10 μ mol/L) and IFN γ (10 ng/mL) or not. GAPDH and LAMINB were used as cytoplasm and nucleus loading control, respectively. (E) *CD274* promoter activity in NCI-H292 cells treated with rosuvastatin (10 μ mol/L) and MVA (0.5 mmol/L) alone or both was detected by dual-luciferase assay. (F, G) The half-life of *CD274* mRNA in HCC827 cells with MVA (0.5 mmol/L) treatment (F) and NCI-H292 cells with rosuvastatin (10 μ mol/L) and MVA alone or both was measured (G). Data are presented as the mean \pm sd of triplicate or quadruplicate independent experiments. Student's *t*-test was used to determine statistical differences (two groups). The data were analyzed by one-way ANOVA with Dunnett's *post hoc* test (more than two groups). ****P* < 0.001; ***P* < 0.01; n.s., not significantly different.

We then examined whether the half-life of *CD274* mRNA was influenced upon MVA modification. As shown in Fig. 4F, the half-life of *CD274* mRNA was significantly increased in HCC827 cells with MVA supply. Furthermore, rosuvastatin significantly shortened the half-life of *CD274* mRNA, which was

reversed by MVA supply (Fig. 4G). Similarly, intervention of HMGCR protein levels also altered the half-life of *CD274* mRNA (Fig. S3E and S3F). Taken together, these findings suggest that MVA regulated the half-life of *CD274* mRNA in tumor cells.

3.5. HuR is involved in MVA mediated CD274 mRNA stability

The 3'-UTR region confers a critical role in mRNA decay depending on the presence of miRNA binding sites and AREs³⁹. Recent studies have demonstrated the importance of 5'-UTR in regulating mRNA stability⁴⁰. To analyze the supposition, we applied luciferase reporter containing the fragment of the 3'-UTR or 5'-UTR of human *CD274* to luciferase assay. The results showed that MVA addition or rosuvastatin administration significantly changed the expression of the *CD274* 3'-UTR luciferase reporter, whereas no significant effect was found on 5'-UTR luciferase reporter (Fig. 5A). Similarly, overexpression or knockdown HMGCR protein also altered the expression of the

CD274 3'-UTR luciferase reporter (Supporting Information Fig. S4A).

ARE and AU-rich element RNA-binding proteins (AUBPs) located in the 3'-UTR region of mRNA have been confirmed to regulate mRNA stability⁴¹. Previous study showed that oncogenic RAS signaling in lung adenocarcinoma induced Tristetraprolin (TTP) phosphorylation in the 3'-UTR of *CD274* mRNA, thereby enhancing *CD274* mRNA stability⁴². In addition, type 1 angiotensin II receptor signaling activation was reported to stabilize *CD274* mRNA through HuR, resulting in PD-L1 up-regulation in NSCLC cells⁴³. To explore whether AUBPs are involved in this process, we knocked down currently identified AUBPs by siRNA, including HuR, KSRP, RHAU, ARE-associated factor 1 (AUF1),

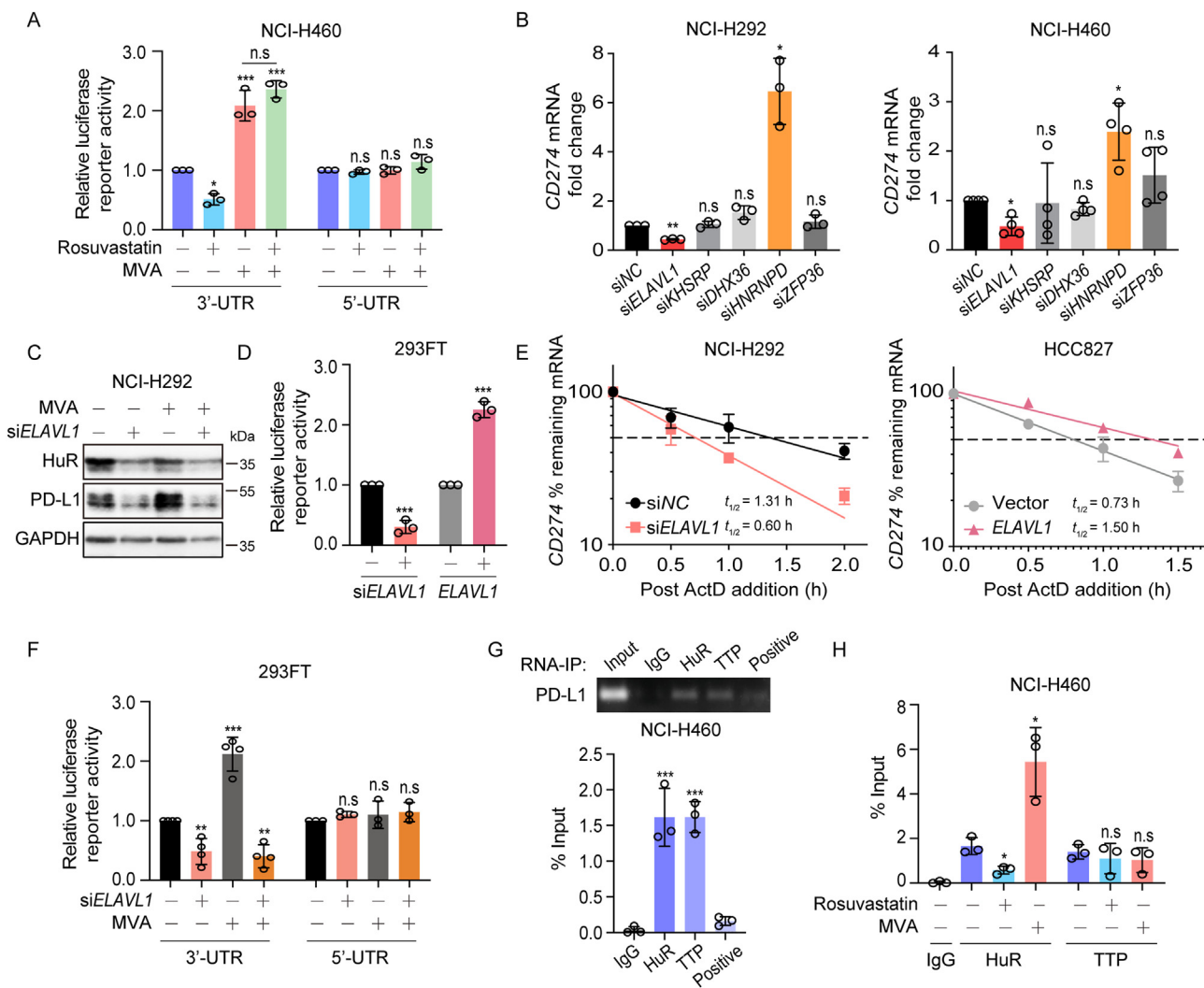


Figure 5 HuR is involved in MVA mediated *CD274* mRNA stability. (A) *CD274* 3'-UTR and 5'-UTR activity in NCI-H460 cells treated with rosuvastatin (10 μ mol/L) and MVA (0.5 mmol/L) alone or both were detected by dual-luciferase assay. (B) qRT-PCR analysis of *CD274* mRNA levels in NCI-H292 (left) and NCI-H460 (right) with transient AUBPs knockdown. (C) Western blot of NCI-H292 cells treated with MVA (0.5 mmol/L) alone or in the presence of HuR silencing. (D) Dual-luciferase assay of HEK 293FT cells with transient HuR knockdown or overexpression. (E) qRT-PCR analysis of *CD274* mRNA stability in cells transfected with *ELAVL* siRNA (left) and Flag-*ELAVL* (right) after the treatment of actinomycin D (5 μ g/mL). (F) *CD274* 3'-UTR and 5'-UTR activity in HEK 293FT cells with MVA (0.5 mmol/L) alone or in the presence of *ELAVL* siRNA were detected by dual-luciferase assay. (G) qPCR and qRT-PCR analysis of the binding of HuR and TTP on the *CD274* 3'-UTR regions via RIP from NCI-H460 cells. (H) RIP was performed with anti-HuR or anti-TTP followed by qRT-PCR analysis of *CD274* 3'-UTR regions in NCI-H460 cells treated with MVA (0.5 mmol/L) or rosuvastatin (10 μ mol/L). Data are presented as the mean \pm sd of triplicate or quadruplicate independent experiments. Student's *t*-test was used to determine statistical differences (two groups). The data were analyzed by one-way ANOVA with Dunnett's *post hoc* test (more than two groups). ****P* < 0.001; ***P* < 0.01; **P* < 0.05; n.s., not significantly different.

and TTP³⁹. We found that knockdown of HuR, a factor stabilizes mRNA, decreased *CD274* mRNA levels, while knockdown of TTP and AUF-1, the factors promote mRNA degradation, increased *CD274* mRNA levels (NCI-H292 is *KRAS* wild-type cell line) (Fig. 5B and Fig. S4B), indicating that HuR, AUF1 and TTP were the potential AUBPs modulating *CD274* mRNA stability. Further, to identify which AUBP is involved in MVA mediated in *CD274* mRNA stability, we analyzed the expression of PD-L1 in the absence of AUBPs. Up-regulation of PD-L1 caused by MVA was eliminated when HuR was knocked down (Fig. 5C), while reintroducing the siRNA-resistant *ELAVL* cDNA into si*ELAVL*-treated cells strikingly restored the promotion of PD-L1 expression by MVA (Fig. S4C). However, knockdown of TTP and AUF-1 protein didn't affect the regulation of PD-L1 by rosuvastatin and MVA (Fig. S4D). We further confirmed the role of HuR in improving *CD274* mRNA levels (Fig. S4E), the expression of *CD274* 3'-UTR luciferase reporter (Fig. 5D) and mRNA stability (Fig. 5E). Crucially, the up-regulated effect of MVA on the expression of *CD274* 3'-UTR luciferase reporter was abolished after HuR knockdown (Fig. 5F). By RIP experiments, we confirmed that both HuR and TTP were bound to *CD274* mRNA 3'-UTR domain (Fig. 5G). However, the blunted binding between *CD274* 3'-UTR domain and HuR but not TTP was found upon rosuvastatin treatment (Fig. 5H). Taken together, these results suggest that MVA improved *CD274* mRNA stability through HuR.

3.6. MVA enhances the anti-tumor effect of PD-1/PD-L1 blockade

Since our study showed that MVA stabilized *CD274* mRNA by promoting the binding of HuR to *CD274* mRNA, we speculated that supplementation of MVA might sensitize tumors to anti-PD-1/PD-L1 therapy *in vivo*. We therefore used CT26 mouse model, an immunocompetent mouse model with efficient PD-1/PD-L1 interaction⁴⁴, which is widely used for anti-PD-(L)1 based studies⁴⁵. Mice bearing CT26 colon cancer were supplemented with MVA by intraperitoneal injection daily to induce high plasma MVA levels²⁶ and administered with anti-mouse PD-L1 antibody twice a week to investigate the sensitization of MVA on anti-PD-L1 therapy (Fig. 6A). MVA addition alone induced a slight increase in tumor growth, and combination of MVA and anti-PD-L1 exhibited a synergistic effect in inhibiting tumor growth than anti-PD-L1 alone (Fig. 6B). Strikingly, combination of MVA and anti-PD-L1 further enhanced the infiltration levels of CD8⁺ and CD3⁺ T cells in TME (Fig. 6C and D). Similar to *in vitro* results, the expression of PD-L1 in tumor cells was increased after MVA administration (Fig. 6E). ELISA analysis showed that cytotoxic activity of CD8⁺ T cells was slightly inhibited by MVA as indicated by decreased secretion of IFN γ , IL-2 and TNF α , while the cytokines were significantly up-regulated in combination of MVA and anti-PD-L1 therapy compared with anti-PD-L1 treatment (Fig. 6F). Collectively, the above results indicated that MVA up-regulated the PD-L1 expression *in vivo*, and provided a potential benefit for PD-1/PD-L1 blockade.

Furthermore, to confirm that the regulation of PD-L1 by MVA was dependent on MVA–HuR–PD-L1 axis, we constructed *Elavl1* knockout CT26 cells with two targeted sgRNAs. As shown in Fig. 6G, the *Elavl1* knockout could significantly down-regulate PD-L1 expression in CT26 cells. Subsequently, we established #1 sgRNA generated *Elavl1* knockout CT26 cells *in vivo* model to

evaluate the efficacy of combined therapy. Interestingly, the mice seeded the *Elavl1* knockout cells exhibited slower growth of tumor compared to *Elavl1* wildtype tumor cells (Fig. 6H and B). Recent studies have shown that HuR is overexpressed in most cancers to stabilize and increase the translation of numerous pro-survival mRNAs involved in the pathogenesis of tumors, which is now recognized as a potential therapeutic target^{46,47}. Therefore, knocking out *Elavl1* has a certain inhibitory effect on tumor growth. Furthermore, compared with anti-PD-L1 group, the synergistic effect in inhibiting tumor growth of combination of MVA and anti-PD-L1 was abolished in *Elavl1* knockout CT26 cells (Fig. 6H). Similarly, combination of MVA and anti-PD-L1 did not further enhance the infiltration levels of CD8⁺ and CD3⁺ T cells in TME (Fig. 6J), and the up-regulation of PD-L1 in tumor cells also disappeared (Fig. 6K). Overall, these results indicated that the efficacy of combined therapy of MVA and anti-PD-L1 was greatly dependent on MVA–HuR–PD-L1 axis.

4. Discussion

The significance of metabolites in modulating immunotherapeutic responses is appreciated recently, and metabolic intervention is expected to provide a strategy to improve the efficacy of immunotherapy^{1,48}. Our study investigated that NSCLC patients with high plasma MVA level had a better clinical efficacy of anti-PD-1 therapy, which was related with PD-L1 expression in tumor. Further mechanistic studies revealed that MVA stabilized *CD274* mRNA in tumor cells by enhancing affinity between ARE-binding protein HuR and 3'-UTR regions of *CD274* mRNA. *In vivo* supplementation with MVA enhances the anti-tumor effect of anti-PD(L)1 antibody (Fig. 7).

Recent studies have focused on the impacts of MVA pathway metabolites on tumor immune microenvironment. Cholesterol, MVA metabolism derivatives, has recently been investigated to induce the up-regulation of immunosuppressive molecules such as PD-1, 2B4 and TIM-3 in CD8⁺ T cells in an ER-stress-XBP1-dependent manner, which mediates CD8⁺ T cells exhaustion and promotes tumor growth²². Moreover, a lipid metabolic-inflammatory circuit is linked to the induction of type I IFN-mediated inflammation with perturbations in the pool size of synthesized cholesterol⁴⁹. MVA pathway inhibitors are confirmed to induce the depletion of prenyl pyrophosphates, thus acquiring the capability to potentially activate IL-2-primed NK cells⁵⁰. Interrupting the geranylgeranylation of small GTPase, such as Rab5 in antigen presenting cells, results in enhanced antigen presentation and T cell activation⁵¹. In addition, recent studies have found that GM-CSF could promote glycolysis and stimulate lipogenesis by increasing HMGCR expression in macrophages, which affects macrophage activation in inflammation⁵². Similarly, dendritic cells maturation has been shown to be dependent on glycolysis-driven lipogenesis by MVA metabolism⁵³. Previous studies have revealed the role of MVA metabolism in tumor immunity, however, most studies focused on the direct influence on immune cells. Whether MVA metabolism can affect the immune microenvironment and the efficacy of immunotherapy through tumor cells is still unclear.

Our findings demonstrated that MVA inhibited the production of MVA to down-regulate PD-L1 expression in tumor cells. Similarly, Choe et al.⁵⁴ found that statins could improve the therapeutic efficacy of PD-L1 mAb by reducing the PD-L1 levels in tumor cells and extracellular vesicles. Simvastatin was

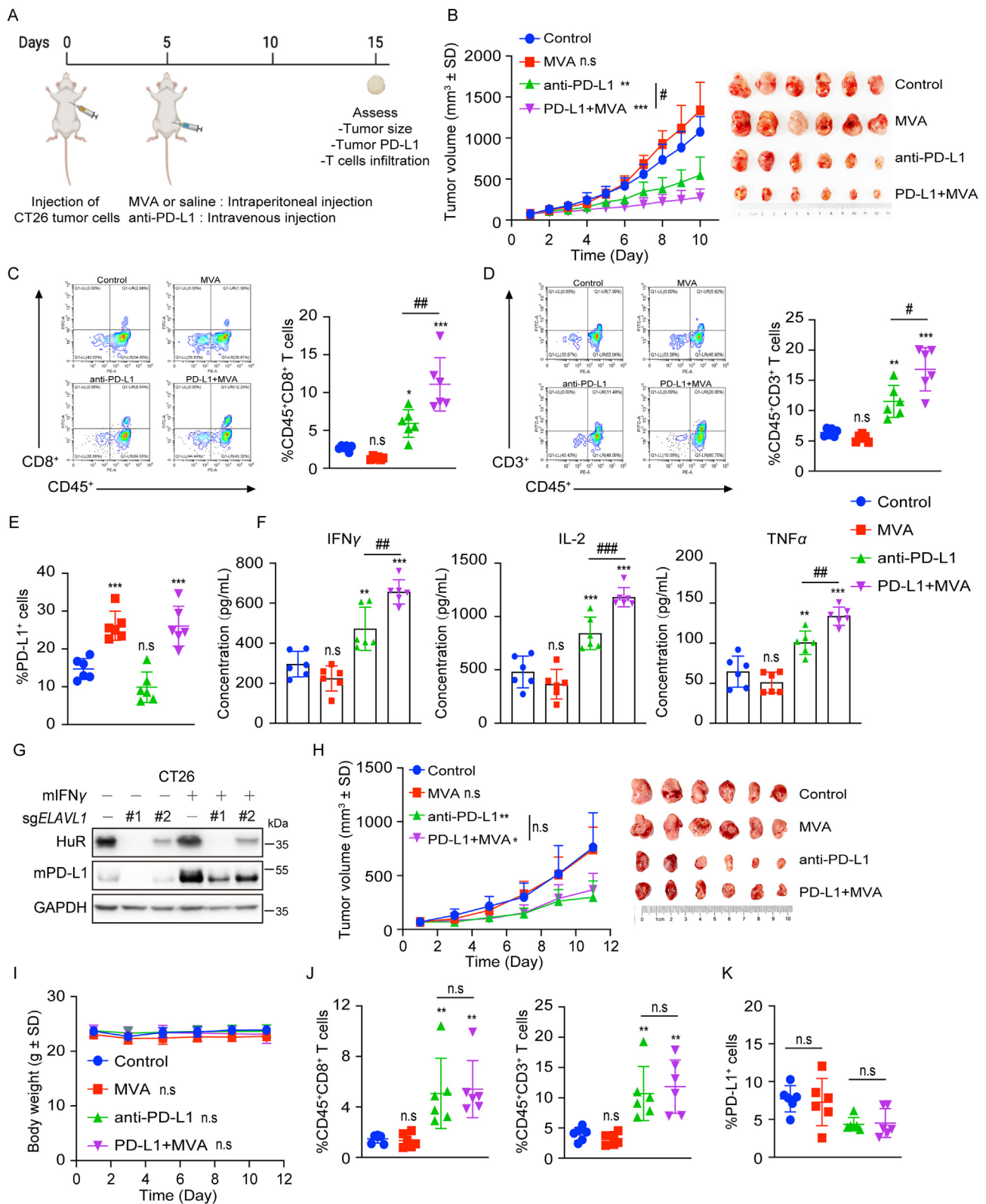


Figure 6 MVA enhances the anti-tumor effect of PD-1/PD-L1 blockade. (A) Schematic illustration of the experimental procedure. The mice bearing tumor were intraperitoneally injected with MVA daily (100 mg/kg) and tail vein injected with anti-PD-L1 (5 mg/kg) twice a week ($n = 6$). (B) The average tumor volume of each group was depicted over time. Data are represented as mean \pm sd. (C, D) Tumor infiltrating CD8⁺ (C) and CD3⁺ (D) T cells in the tumors of each group were analyzed by flow cytometry. Representative flow cytometry images of tumors were presented on the left. (E) Cell-surface PD-L1 expression was determined by flow cytometry in mouse tumor tissues of each group. (F) The production of IFN γ , IL-2 and TNF α in the tumors of each group were evaluated by ELISA assay. (G) Western blot to detect the expression of PD-

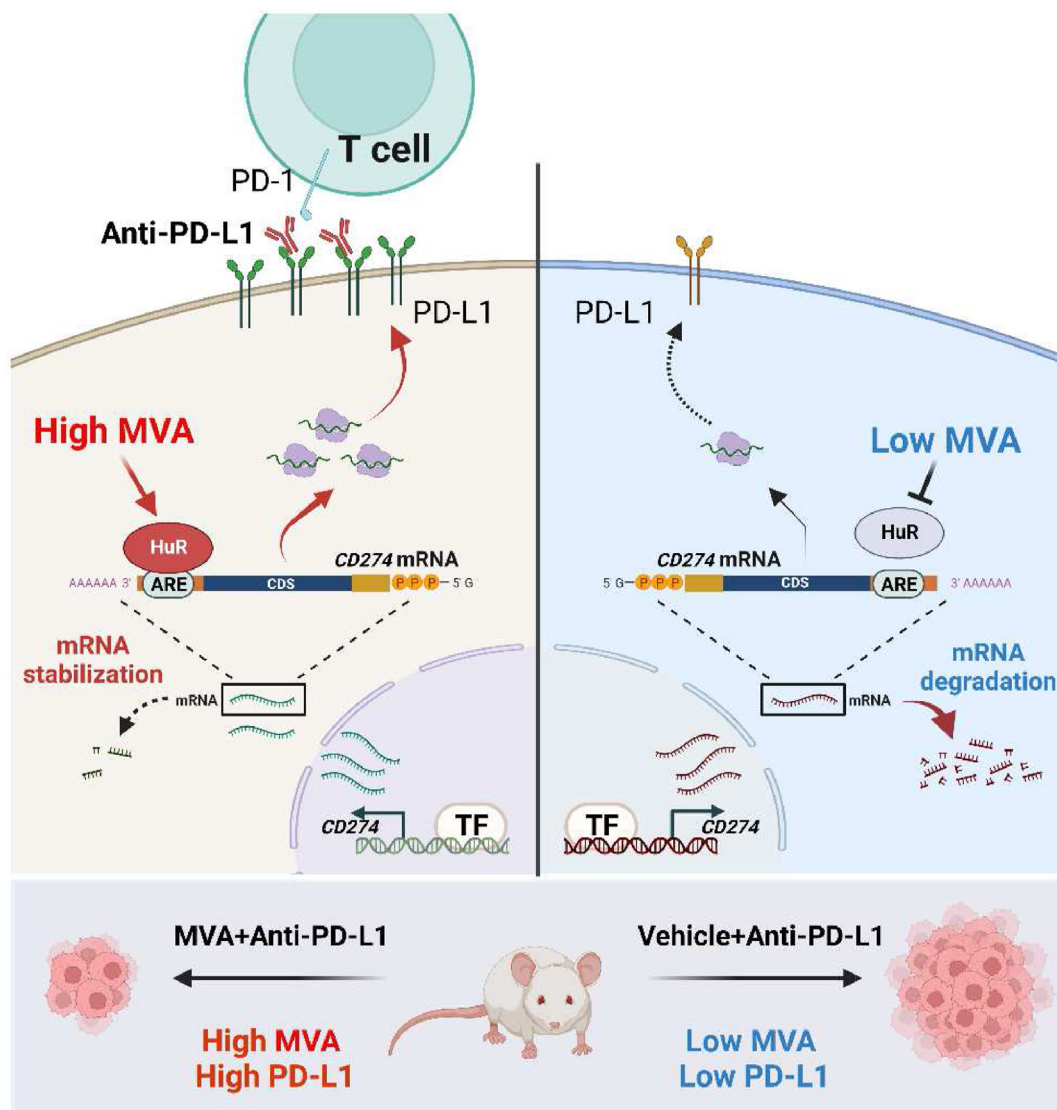


Figure 7 Scheme for the effect of MVA on stabilizing the *CD274* mRNA. (A) Tumor cell with high MVA levels or supplemented MVA can significantly up-regulate PD-L1 expression by maintaining the affinity of HuR and *CD274* mRNA 3'-UTR regions, thereby stabilizing its mRNA. (B) Tumor cell with low MVA levels or inhibited MVA has blunted affinity of HuR and *CD274* mRNA 3'-UTR regions, resulting to mRNA rapid degradation. (C) Supplementing MVA in combination with anti-PD-L1 in syngeneic mouse model can significantly up-regulate the expression of PD-L1 in tumor cells and enhance the anti-tumor effect of anti-PD-L1 treatment.

investigated to down-regulate PD-L1 transcription by inhibiting the expression of lncRNA *SNHG29* and enhance the effects of PD-L1 mAb in animal models⁵⁵. Furthermore, statins can be used as vaccine adjuvants to increase the efficacy of immune checkpoint inhibitors by increasing antigen presentation and prolonging antigen retention⁵⁶. An integrated analysis of concomitant medications from PD-1/PD-L1 checkpoint inhibitors in clinic practice found that baseline statins were confirmed to prolong the overall survival of patients received PD-1 mAb therapy, but showed no

statistically significant difference in PFS⁵⁷. Additional systematic evaluation and meta-analysis of the effect of statins on immune checkpoint inhibitor outcomes indicated that statins could improve PFS and OS of PD-1/PD-L1 mAb therapy⁵⁸. However, some studies have shown that statins were investigated to be independently related to an increased objective response rate^{59,60}. A differential analysis of other medications on oncological outcomes of patients with NSCLC treated with pembrolizumab indicated that no association with clinical outcomes was found according to

L1 and HuR with or without mouse IFN γ (10 ng/mL) treatment in two targeted sgRNAs generated *Elavl1* knockout CT26 cells. (H, I) The average tumor volume and body weight of each group mice seeded the *Elavl1* knockout cells was depicted over time. Data are represented as mean \pm sd. (J) Tumor infiltrating CD8⁺ (left) and CD3⁺ (right) T cells in the tumors of each group were analyzed by flow cytometry. (K) Cell-surface PD-L1 expression was determined by flow cytometry in mouse tumor tissues of each group. Student's *t*-test was used to determine Statistical differences (two groups). The data were analyzed by one-way ANOVA with Dunnett's *post hoc* test (more than two groups). ****P* < 0.001; ***P* < 0.01; **P* < 0.05; ###*P* < 0.001; ##*P* < 0.01; #*P* < 0.05; n.s, not significantly different.

baseline statin with the pembrolizumab cohort. Above all, statins may be a combination strategy for cancer immunotherapy, but still need to be further confirmed.

So far, the most well studied class of mRNA stability element is the ARE. This diverse sequence element is investigated in the 3'-UTR of many transcripts encoding cytokines, transcription factors and proto-oncogenes⁶¹. Recent studies demonstrated that stabilization of *CD274* mRNA contributes to its expression. Oncogenic RAS signaling in NSCLC increases *CD274* mRNA stability *via* inducing phosphorylation and inhibition of TTP⁴². Besides, type 1 angiotensin II receptor signaling was reported to enhance HuR binds to and stabilizes the *CD274* mRNA⁴³. Our study show that MVA can significantly affect the stability of *CD274* mRNA and activity of *CD274* 3'-UTR luciferase reporter. Consistent with previous studies, we found that both TTP and HuR can regulate *CD274* mRNA stability. Interestingly, our studies show that knockdown of the ARE-binding protein AUF-1 also can significantly up-regulate *CD274* mRNA levels. However, further studies suggested that TTP and AUF-1 were not involved in the regulation of *CD274* mRNA stability by MVA, and demonstrated that MVA can enhance the binding ability of HuR to *CD274* mRNA, thereby stabilizing PD-L1 expression in tumor cells. Meanwhile, it remains unclear how MVA affects the affinity of the HuR to 3'-UTR region of *CD274* mRNA. Recently, Wang et al.⁶² found that cholesterol could directly bind to the CRAC motifs in the transmembrane domain of PD-L1 and enhance the stability of cell-surface PD-L1. However, their data showed that supplementation of cholesterol did not have significant impact on total PD-L1 expression. They also showed that statins could significantly reduce PD-L1 expression, which was consistent with our study. Furthermore, previous studies have shown that small GTPases such as RAS⁶³ and RAC⁶⁴ can regulate mRNA stability by affecting the post-translational modification and nucleocytoplasmic shuttling ability of ARE-binding proteins. Other studies have demonstrated that RhoA is required for the formation of P bodies in the cytoplasm, a key site of mRNA degradation⁶⁵. Detailed mechanisms whether MVA can regulate the isoprenylation of small GTPases, thus affecting post-translational modification of HuR or relating to the formation of P bodies in the cytoplasm, remain to be investigated.

5. Conclusions

This study demonstrates a previously unappreciated role of MVA in modulating anti-tumor immunity, and identifies the importance of the MVA in stabilizing PD-L1 expression in tumor cells. NSCLC patients with high plasma MVA levels may account for higher PD-L1 expression in tumor and a better response with immune checkpoint blockade. Furthermore, our study provided a rationale to explore the application of MVA supplement as an immunosensitizer in NSCLC.

Acknowledgments

This work was supported by National Natural Science Foundation of China (No. 81930102 to Bo Yang, No. 82104196 to Xi Chen, No. 82273949 to Ling Ding) and Key R&D Program of Zhejiang (No. 2022C03143 to Qinjie Weng, China).

Author contributions

Wenxin Zhang and Xiaohui Pan contributed to the design, performed experiments of the work and wrote the manuscript; Hongjie Guo, Mingming Zheng, Xi Chen, Honghai Wu and Qiaojun He contributed to the acquisition of the work, performed statistical analysis and revised the article; Yanjun Xu and Fengming Luan contributed to the patient samples collection of the work and assisted in patients' immunotherapy outcomes and tumor PD-L1 IHC analysis; Ling Ding and Bo Yang contributed to the conception of the work and provided project supervision.

Conflicts of interest

The authors declare no competing interests.

Appendix A. Supporting information

Supporting data to this article can be found online at <https://doi.org/10.1016/j.apsb.2023.04.002>.

References

- Xia L, Oyang L, Lin J, Tan S, Han Y, Wu N, et al. The cancer metabolic reprogramming and immune response. *Mol Cancer* 2021; **20**:28.
- Certo M, Tsai CH, Pucino V, Ho PC, Mauro C. Lactate modulation of immune responses in inflammatory *versus* tumour microenvironments. *Nat Rev Immunol* 2021; **21**:151–61.
- Wang D, Cabalag CS, Clemons NJ, DuBois RN. Cyclooxygenases and prostaglandins in tumor immunology and microenvironment of gastrointestinal cancer. *Gastroenterology* 2021; **161**:1813–29.
- Brand A, Singer K, Koehl GE, Kolitzus M, Schoenhammer G, Thiel A, et al. LDHA-associated lactic acid production blunts tumor immunosurveillance by T and NK cells. *Cell Metab* 2016; **24**:657–71.
- Bottcher JP, Bonavita E, Chakravarty P, Bleses H, Cabeza-Cabrerizo M, Sammicheli S, et al. NK cells stimulate recruitment of cDC1 into the tumor microenvironment promoting cancer immune control. *Cell* 2018; **172**:1022–1037.e14.
- Feng J, Yang H, Zhang Y, Wei H, Zhu Z, Zhu B, et al. Tumor cell-derived lactate induces TAZ-dependent upregulation of PD-L1 through GPR81 in human lung cancer cells. *Oncogene* 2017; **36**:5829–39.
- Bonavita E, Bromley CP, Jonsson G, Pelly VS, Sahoo S, Walwyn-Brown K, et al. Antagonistic inflammatory phenotypes dictate tumor fate and response to immune checkpoint blockade. *Immunity* 2020; **53**:1215–1229.e8.
- Li N, Kang Y, Wang L, Huff S, Tang R, Hui H, et al. ALKBH5 regulates anti-PD-1 therapy response by modulating lactate and suppressive immune cell accumulation in tumor microenvironment. *Proc Natl Acad Sci U S A* 2020; **117**:20159–70.
- Yuan XL, Chen L, Li MX, Dong P, Xue J, Wang J, et al. Elevated expression of Foxp3 in tumor-infiltrating Treg cells suppresses T-cell proliferation and contributes to gastric cancer progression in a COX-2-dependent manner. *Clin Immunol* 2010; **134**:277–88.
- Geiger R, Rieckmann JC, Wolf T, Basso C, Feng Y, Fuhrer T, et al. L-Arginine modulates T cell metabolism and enhances survival and anti-tumor activity. *Cell* 2016; **167**:829–842.e13.
- St Paul M, Saibil SD, Han S, Israni-Winger K, Lien SC, Laister RC, et al. Coenzyme A fuels T cell anti-tumor immunity. *Cell Metab* 2021; **33**:2415–2427.e6.

12. Kumagai S, Koyama S, Itahashi K, Tanegashima T, Lin YT, Togashi Y, et al. Lactic acid promotes PD-1 expression in regulatory T cells in highly glycolytic tumor microenvironments. *Cancer Cell* 2022;**40**:201–218.e9.
13. Prima V, Kaliberova LN, Kaliberov S, Curiel DT, Kusmartsev S. COX2/mPGES1/PGE2 pathway regulates PD-L1 expression in tumor-associated macrophages and myeloid-derived suppressor cells. *Proc Natl Acad Sci U S A* 2017;**114**:1117–22.
14. Chen Z, Chen Y, Peng L, Wang X, Tang N. 2,5-Dimethylcelecoxib improves immune microenvironment of hepatocellular carcinoma by promoting ubiquitination of HBx-induced PD-L1. *J Immunother Cancer* 2020;**8**:e001377.
15. Byun JK, Park M, Lee S, Yun JW, Lee J, Kim JS, et al. Inhibition of glutamine utilization synergizes with immune checkpoint inhibitor to promote antitumor immunity. *Mol Cell* 2020;**80**:592–606.e8.
16. Lv H, Lv G, Chen C, Zong Q, Jiang G, Ye D, et al. NAD⁺ metabolism maintains inducible PD-L1 expression to drive tumor immune evasion. *Cell Metab* 2021;**33**:110–127.e5.
17. Mullen PJ, Yu R, Longo J, Archer MC, Penn LZ. The interplay between cell signalling and the mevalonate pathway in cancer. *Nat Rev Cancer* 2016;**16**:718–31.
18. Wang M, Casey PJ. Protein prenylation: unique fats make their mark on biology. *Nat Rev Mol Cell Biol* 2016;**17**:110–22.
19. Cheng C, Ru P, Geng F, Liu J, Yoo JY, Wu X, et al. Glucose-mediated N-glycosylation of SCAP is essential for SREBP-1 activation and tumor growth. *Cancer Cell* 2015;**28**:569–81.
20. Thurnher M, Gruenbacher G. T lymphocyte regulation by mevalonate metabolism. *Sci Signal* 2015;**8**:re4.
21. Du X, Zeng H, Liu S, Guy C, Dhungana Y, Neale G, et al. Mevalonate metabolism-dependent protein geranylgeranylation regulates thymocyte egress. *J Exp Med* 2020;**217**:e20190969.
22. Ma X, Bi E, Lu Y, Su P, Huang C, Liu L, et al. Cholesterol induces CD8⁺ T cell exhaustion in the tumor microenvironment. *Cell Metab* 2019;**30**:143–156.e5.
23. Lei K, Kurum A, Kaynak M, Bonati L, Han Y, Cencen V, et al. Cancer-cell stiffening via cholesterol depletion enhances adoptive T-cell immunotherapy. *Nat Biomed Eng* 2021;**5**:1411–25.
24. Ding L, Chen X, Zhang W, Dai X, Guo H, Pan X, et al. Canagliflozin primes antitumor immunity by triggering PD-L1 degradation in endocytic recycling. *J Clin Invest* 2023;**133**:e154754.
25. Kindt E, Szekely-Klepser G, Fountain ST. The validation of a simple LC/MS/MS method for determining the level of mevalonic acid in human plasma. *Biomed Chromatogr* 2011;**25**:323–9.
26. Wang H, Rong X, Zhao G, Zhou Y, Xiao Y, Ma D, et al. The microbial metabolite trimethylamine N-oxide promotes antitumor immunity in triple-negative breast cancer. *Cell Metab* 2022;**34**:581–594.e8.
27. Shang M, Yang H, Yang R, Chen T, Fu Y, Li Y, et al. The folate cycle enzyme MTHFD2 induces cancer immune evasion through PD-L1 up-regulation. *Nat Commun* 2021;**12**:1940.
28. Li H, Xiao Y, Li Q, Yao J, Yuan X, Zhang Y, et al. The allergy mediator histamine confers resistance to immunotherapy in cancer patients via activation of the macrophage histamine receptor H1. *Cancer Cell* 2022;**40**:36–52.e9.
29. Guan B, Tong J, Hao H, Yang Z, Chen K, Xu H, et al. Bile acid coordinates microbiota homeostasis and systemic immunometabolism in cardiometabolic diseases. *Acta Pharm Sin B* 2022;**12**:2129–49.
30. Niu M, Yi M, Li N, Luo S, Wu K. Predictive biomarkers of anti-PD-1/PD-L1 therapy in NSCLC. *Exp Hematol Oncol* 2021;**10**:18.
31. Gibney GT, Weiner LM, Atkins MB. Predictive biomarkers for checkpoint inhibitor-based immunotherapy. *Lancet Oncol* 2016;**17**:e542–51.
32. Budimir N, Thomas GD, Dolina JS, Salek-Ardakani S. Reversing T-cell exhaustion in cancer: lessons learned from PD-1/PD-L1 immune checkpoint blockade. *Cancer Immunol Res* 2022;**10**:146–53.
33. Wu Y, Yang Z, Cheng K, Bi H, Chen J. Small molecule-based immunomodulators for cancer therapy. *Acta Pharm Sin B* 2022;**12**:4287–308.
34. Ma X, Xiao L, Liu L, Ye L, Su P, Bi E, et al. CD36-mediated ferroptosis dampens intratumoral CD8⁺ T cell effector function and impairs their antitumor ability. *Cell Metab* 2021;**33**:1001–1012.e5.
35. Pan X, Li R, Guo H, Zhang W, Xu X, Chen X, et al. Dihydropyridine calcium channel blockers suppress the transcription of PD-L1 by inhibiting the activation of STAT1. *Front Pharmacol* 2020;**11**:539261.
36. Ding L, Chen X, Xu X, Qian Y, Liang G, Yao F, et al. PARP1 suppresses the transcription of PD-L1 by poly(ADP-ribosyl)ating STAT3. *Cancer Immunol Res* 2019;**7**:136–49.
37. Chen B, Hu J, Hu X, Chen H, Bao R, Zhou Y, et al. DENR controls JAK2 translation to induce PD-L1 expression for tumor immune evasion. *Nat Commun* 2022;**13**:2059.
38. Fan Z, Wu C, Chen M, Jiang Y, Wu Y, Mao R, et al. The generation of PD-L1 and PD-L2 in cancer cells: from nuclear chromatin reorganization to extracellular presentation. *Acta Pharm Sin B* 2022;**12**:1041–53.
39. Schoenberg DR, Maquat LE. Regulation of cytoplasmic mRNA decay. *Nat Rev Genet* 2012;**13**:246–59.
40. Jia L, Mao Y, Ji Q, Dersh D, Yewdell JW, Qian SB. Decoding mRNA translatability and stability from the 5' UTR. *Nat Struct Mol Biol* 2020;**27**:814–21.
41. Garneau NL, Wilusz J, Wilusz CJ. The highways and byways of mRNA decay. *Nat Rev Mol Cell Biol* 2007;**8**:113–26.
42. Coelho MA, de Carne Trecesson S, Rana S, Zecchin D, Moore C, Molina-Arcas M, et al. Oncogenic RAS signaling promotes tumor immunoresistance by stabilizing PD-L1 mRNA. *Immunity* 2017;**47**:1083–1099.e6.
43. Yang K, Zhou J, Chen Y, Chen Y, Chen L, Zhang P, et al. Angiotensin II contributes to intratumoral immunosuppression via induction of PD-L1 expression in non-small cell lung carcinoma. *Int Immunopharmacol* 2020;**84**:106507.
44. Yadav M, Jhunjhunwala S, Phung QT, Lupardus P, Tanguay J, Bumbaca S, et al. Predicting immunogenic tumour mutations by combining mass spectrometry and exome sequencing. *Nature* 2014;**515**:572–6.
45. Zhang J, Bu X, Wang H, Zhu Y, Geng Y, Nihira NT, et al. Cyclin D-CDK4 kinase destabilizes PD-L1 via cullin 3–SPOP to control cancer immune surveillance. *Nature* 2018;**553**:91–5.
46. Wu X, Xu L. The RNA-binding protein HuR in human cancer: a friend or foe?. *Adv Drug Deliv Rev* 2022;**184**:114179.
47. Zhu Y, Yang L, Xu J, Yang X, Luan P, Cui Q, et al. Discovery of the anti-angiogenesis effect of eltrombopag in breast cancer through targeting of HuR protein. *Acta Pharm Sin B* 2020;**10**:1414–25.
48. Biswas SK. Metabolic reprogramming of immune cells in cancer progression. *Immunity* 2015;**43**:435–49.
49. York AG, Williams KJ, Argus JP, Zhou QD, Brar G, Vergnes L, et al. Limiting cholesterol biosynthetic flux spontaneously engages type I IFN signaling. *Cell* 2015;**163**:1716–29.
50. Gruenbacher G, Gander H, Nussbaumer O, Nussbaumer W, Rahm A, Thurnher M. IL-2 costimulation enables statin-mediated activation of human NK cells, preferentially through a mechanism involving CD56⁺ dendritic cells. *Cancer Res* 2010;**70**:9611–20.
51. Nonaka M, Uota S, Saitoh Y, Takahashi M, Sugimoto H, Amet T, et al. Role for protein geranylgeranylation in adult T-cell leukemia cell survival. *Exp Cell Res* 2009;**315**:141–50.
52. Na YR, Gu GJ, Jung D, Kim YW, Na J, Woo JS, et al. GM-CSF induces inflammatory macrophages by regulating glycolysis and lipid metabolism. *J Immunol* 2016;**197**:4101–9.
53. Everts B, Amiel E, Huang SC, Smith AM, Chang CH, Lam WY, et al. TLR-driven early glycolytic reprogramming via the kinases TBK1–IKKε supports the anabolic demands of dendritic cell activation. *Nat Immunol* 2014;**15**:323–32.
54. Choe EJ, Lee CH, Bae JH, Park JM, Park SS, Baek MC. Atorvastatin enhances the efficacy of immune checkpoint therapy and suppresses the cellular and extracellular vesicle PD-L1. *Pharmaceutics* 2022;**14**:1660.
55. Ni W, Mo H, Liu Y, Xu Y, Qin C, Zhou Y, et al. Targeting cholesterol biosynthesis promotes anti-tumor immunity by inhibiting long

- noncoding RNA SNHG29-mediated YAP activation. *Mol Ther* 2021; **29**:2995–3010.
56. Xia Y, Xie Y, Yu Z, Xiao H, Jiang G, Zhou X, et al. The mevalonate pathway is a druggable target for vaccine adjuvant discovery. *Cell* 2018; **175**:1059–1073.e21.
 57. Takada K, Shimokawa M, Takamori S, Shimamatsu S, Hirai F, Tagawa T, et al. A propensity score-matched analysis of the impact of statin therapy on the outcomes of patients with non-small-cell lung cancer receiving anti-PD-1 monotherapy: a multicenter retrospective study. *BMC Cancer* 2022; **22**:503.
 58. Zhang Y, Chen H, Chen S, Li Z, Chen J, Li W. The effect of concomitant use of statins, NSAIDs, low-dose aspirin, metformin and beta-blockers on outcomes in patients receiving immune checkpoint inhibitors: a systematic review and meta-analysis. *Oncoimmunology* 2021; **10**:1957605.
 59. Cortellini A, Di Maio M, Nigro O, Leonetti A, Cortinovis DL, Aerts JG, et al. Differential influence of antibiotic therapy and other medications on oncological outcomes of patients with non-small cell lung cancer treated with first-line pembrolizumab versus cytotoxic chemotherapy. *J Immunother Cancer* 2021; **9**:e002421.
 60. Cortellini A, Tucci M, Adamo V, Stucci LS, Russo A, Tanda ET, et al. Integrated analysis of concomitant medications and oncological outcomes from PD-1/PD-L1 checkpoint inhibitors in clinical practice. *J Immunother Cancer* 2020; **8**:e001361.
 61. Vlasova-St Louis I, Bohjanen PR. Post-transcriptional regulation of cytokine and growth factor signaling in cancer. *Cytokine Growth Factor Rev* 2017; **33**:83–93.
 62. Wang Q, Cao Y, Shen L, Xiao T, Cao R, Wei S, et al. Regulation of PD-L1 through direct binding of cholesterol to CRAC motifs. *Sci Adv* 2022; **8**:eabq4722.
 63. Sheng H, Shao J, Dubois RN. K-Ras-mediated increase in cyclooxygenase 2 mRNA stability involves activation of the protein kinase B1. *Cancer Res* 2001; **61**:2670–5.
 64. Morrison AR, Yarovinsky TO, Young BD, Moraes F, Ross TD, Ceneri N, et al. Chemokine-coupled beta2 integrin-induced macrophage Rac2–Myosin IIA interaction regulates VEGF-A mRNA stability and arteriogenesis. *J Exp Med* 2014; **211**:1957–68.
 65. Takahashi S, Sakurai K, Ebihara A, Kajihio H, Saito K, Kontani K, et al. RhoA activation participates in rearrangement of processing bodies and release of nucleated AU-rich mRNAs. *Nucleic Acids Res* 2011; **39**:3446–57.